Astronomy & Astrophysics manuscript no. GRB111117A_diff

Saturday 25th November, 2017

The host galaxy of the short GRB 111117A at $z = 2.211$: impact on the short GRB redshift distribution and progenitor channels*

J. Selsing[1], T. Krühler[2], D. Malesani[1], P. D'Avanzo[3], S. Schulze[4, 5, 6], S. D. Vergani[3, 7], J. Palmerio[8], J. Japelj[9], B. Milvang-Jensen[1], D. Watson[1], P. Jakobsson[10], J. Bolmer[2], Z. Cano[11], S. Covino[3], V. D'Elia[12, 13], A. de Ugarte Postigo[11, 1], J. P. U. Fynbo[1], A. Gomboc[14], K. E. Heintz[10, 1], L. Kaper[9], A. J. Levan[15], S. Piranomonte[12], G. Pugliese[9], R. Sánchez-Ramírez[11, 16], M. Sparre[1, 17], N. R. Tanvir[18], C. C. Thöne[11], and K. Wiersema[18]

*Based on observations collected at ESO/VLT under programme 088.A-0051 and 091.D-0904, at TNG under programme A24TAC_38, at Gemini North under programme GN-2011B-Q-10 and GTC under programme GTC43-11B.

[1] Dark Cosmology Centre, Niels Bohr Institute, University of Copenhagen, Juliane Maries Vej 30, 2100 København Ø, Denmark

[2] Max-Planck-Institut für extraterrestrische Physik, Giessenbachstraße, 85748 Garching, Germany

[3] INAF - Osservatorio Astronomico di Brera, via E. Bianchi 46, I-23807, Merate (LC), Italy

[4] Instituto de Astrofísica, Facultad de Física, Pontificia Universidad Católica de Chile, Vicuña Mackenna 4860, 7820436 Macul, Santiago, Chile

[5] Millennium Institute of Astrophysics, Vicuña Mackenna 4860, 7820436 Macul, Santiago, Chile

[6] Department of Particle Physics and Astrophysics, Faculty of Physics, Weizmann Institute of Science, Rehovot 76100, Israel

[7] GEPI, Observatoire de Paris, PSL Research University, CNRS, Place Jules Janssen, 92190 Meudon, France

[8] Sorbonne Universités, UPMC Univ. Paris 6 et CNRS, UMR 7095, Institut d'Astrophysique de Paris, 98 bis bd Arago, 75014 Paris, France

[9] Anton Pannekoek Institute for Astronomy, University of Amsterdam, Science Park 904, 1098 XH Amsterdam, The Netherlands

[10] Centre for Astrophysics and Cosmology, Science Institute, University of Iceland, Dunhagi 5, 107 Reykjavík, Iceland

[11] Instituto de Astrofísica de Andalucía (IAA-CSIC), Glorieta de la Astronomía s/n, E-18008, Granada, Spain

[12] INAF-Osservatorio Astronomico di Roma, Via Frascati 33, I-00040 Monteporzio Catone, Italy

[13] ASI-Science Data Centre, Via del Politecnico snc, I-00133 Rome, Italy

[14] Centre for Astrophysics and Cosmology, University of Nova Gorica, Vipavska 13, 5000 Nova Gorica, Slovenia.

[15] Department of Physics, University of Warwick, Coventry CV4 7AL, UK

[16] Istituto de Astrofisica e Planetologia Spaziali, INAF, Via Fosso del Cavaliere 100, I-00133 Roma, Italy

[17] Heidelberger Institut für Theoretische Studien, Schloss-Wolfsbrunnenweg 35, 69118 Heidelberg, Germany

[18] Department of Physics & Astronomy and Leicester Institute of Space & Earth Observation, University of Leicester, University Road, Leicester, LE1 7RH, UK

Received/ accepted

ABSTRACT

It is notoriously difficult to localize short γ-ray bursts (sGRBs) and their hosts to measure their redshifts. These measurements, however, are critical to constrain the nature of sGRB progenitors, their redshift distribution and the r-process element enrichment history of the universe. Here, we present spectroscopy of the host galaxy of GRB 111117A and measure its redshift to be $z = 2.211$. This makes GRB 111117A the most distant high-confidence short duration GRB detected to date.

Our spectroscopic redshift supersedes a lower, previously estimated photometric redshift value for this burst.

We use the spectroscopic redshift, as well as new imaging data to constrain the nature of the host galaxy and the physical parameters of the GRB. The rest-frame X-ray derived hydrogen column density, for example, is the highest compared to a complete sample of sGRBs and seems to follow the evolution with redshift as traced by the hosts of long GRBs.

The host lies in the brighter end of the expected sGRB host brightness distribution at z = 2.211, and is actively forming stars. Using the observed sGRB host luminosity distribution, we find that between 43 and 71 per cent of all *Swift*-detected sGRBs have too faint hosts at $z \sim 2$ to allow for a secure redshift determination. This implies that the measured sGRB redshift distribution could be incomplete at high redshift. The large z of GRB 111117A is evidence against a lognormal delay-time model for sGRBs through the predicted redshift distribution of sGRBs, which is very sensitive to high-z sGRBs.

From the age of the universe at the time of GRB explosion, an initial neutron star (NS) separation of $a_0 < 3.1\ R_\odot$ is required in the case where the progenitor system is a circular pair of inspiralling NSs. This constraint excludes some of the longest sGRB formation channels for this burst.

Key words. gamma-ray burst: individual: GRB 111117A – gamma-ray burst: general – galaxies: high-redshift – binaries: general – X-rays: bursts – techniques: imaging spectroscopy

1. Introduction

There is mounting evidence that short-duration γ-ray bursts **(sGRBs)** come from the merger of **a neutron star (NS)**, either with another NS, or a black hole, due to their apparent association with kilonovae (**Barnes & Kasen 2013**, **Tanvir et al. 2013**, **Berger et al. 2013**, **Yang et al. 2015**, **Jin et al. 2016**, **Rosswog et al. 2017**). **This association was recently confirmed by the simultaneous and co-spatial detection of gravitational waves (GWs) from a binary neutron star merger and a sGRB (Abbott et al. 2017b, Goldstein et al. 2017, Savchenko et al. 2017).** The absence of associated supernovae in deep searches (e.g. Hjorth et al. 2005b, Fox et al. 2005, Hjorth et al. 2005a, Kann et al. 2011) supports this idea and distinguishes the physical origin of sGRBs from their long-duration counterparts, (albeit see also Fynbo et al. 2006, Della Valle et al. 2006, Gal-Yam et al. 2006).

The classification of GRBs in two groups initially comes from the bimodal distribution of burst duration and spectral hardness **in the BATSE sample** (**Kouveliotou et al. 1993**), where the duration $T_{90} < 2$ **s** has been regarded as the dividing line between long and short GRBs. Additionally, it has been found for **long GRBs (lGRBs)** that there is a spectral lag in the arrival-time of photons, with the most energetic ones arriving first. This lag is consistent with zero for sGRBs (Norris & Bonnell 2006). Because both populations have continuous, overlapping distributions in their observables and because telescopes observe in differing bands, it is difficult to impose a single demarcation criterion between the two classes. For this reason, the distinction between long and short GRBs is preferably based on a combination of **the** high-energy properties (**Zhang et al. 2009**, **Kann et al. 2011**, **Bromberg et al. 2012**, **2013**).

The *Swift* satellite (Gehrels et al. 2004) greatly improved the understanding of sGRB progenitors thanks to its quick localization capability. The bulk of these localizations have associated galaxies at relatively low redshifts with a median redshift of $z \sim 0.5$ (Berger 2014)**. Unlike lGRBs, sGRB afterglows are faint making absorption spectroscopy often ineffective. Therefore,** most of these measurements come from the associated hosts **and is potentially** biased towards lower redshifts. **Additionally, because the *Swift* sensitivity to sGRB decreases sharply with redshift (Behroozi et al. 2014), the intrinsic redshift distribution of sGRBs is largely unknown at higher redshifts.**

The host galaxies of sGRBs are diverse. They are more massive and less actively star-forming on average than lGRB hosts (Fong et al. 2013), while in some cases, no host galaxy can be identified above **the** detection threshold of deep follow-up observations (Berger 2010, Tunnicliffe et al. 2014). Together with their position within their hosts (Fong & Berger 2013), this suggests a progenitor system that can be very long lived in comparison to lGRBs, **with the** host stellar mass **affecting the sGRB rates more than the** star-formation rate (SFR) **(Berger 2014)**.

The electromagnetic signals from sGRBs are a promising channel to accurately localize NS mergers (**Ghirlanda et al. 2016**)**. This epochal breakthrough occurred recently when the first NS-NS GW event ever was detected by LIGO/Virgo (GW 170817) and associated to the weak sGRB 170817A detected by the *Fermi* and INTEGRAL satellites (Abbott et al. 2017b, Goldstein et al. 2017, Savchenko et al. 2017)**. The simultaneous detection of a sGRB and a GW **provides new** promising ways to constrain the binary inclination angle **(Arun et al. 2014, Abbott et al. 2017b)** and measure cosmological distances **(Nissanke et al. 2010, Abbott et al. 2017a)**.

The total **lifetime** of NS binaries depends on their orbit, mass, spin, initial separations and subsequent inspiral times. The delay time from formation to explosion impacts the timing and distribution of the enrichment of the ISM with heavy r-process elements (van de Voort et al. 2014, Wallner et al. 2015, Ji et al. 2016). Some limits can be calculated using host galaxy star-formation history models and spatial distribution of sGRBs within their hosts (Berger 2014). The most distant cosmological bursts, however, offer direct, hard limits on the coalescence time scales.

We here present a spectrum of the host galaxy of the short GRB 111117A ($T_{90} = 0.46$ s) and measure its redshift to be $z = 2.211$. This value is significantly higher than the previously estimated redshift based on photometric studies (Margutti et al. 2012, Sakamoto et al. 2013). We present the GRB's rest frame properties based on this new distance compared to previous analyses and revisit the host properties derived from the new solution to the spectral energy distribution (SED) fit. While no optical afterglow was detected, the excellent localization from a detection of the X-ray afterglow by the *Chandra* X-ray Observatory allows us to discuss the positioning and environmental properties of this remarkably distant sGRB. We use the ΛCDM cosmology

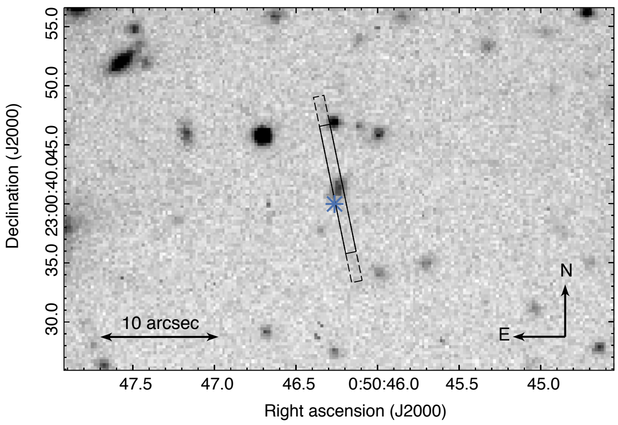

Fig. 1. FORS2 *R*-**band** imaging of the field of GRB 111117A with the X-shooter slit overlaid. The slit position represents 4 epochs of spectroscopic observations taken at similar position angles. The corresponding photometry is shown in Fig. 3. The blue asterisk indicates the GRB position as derived from the *Chandra* observations in Sakamoto et al. (2013).

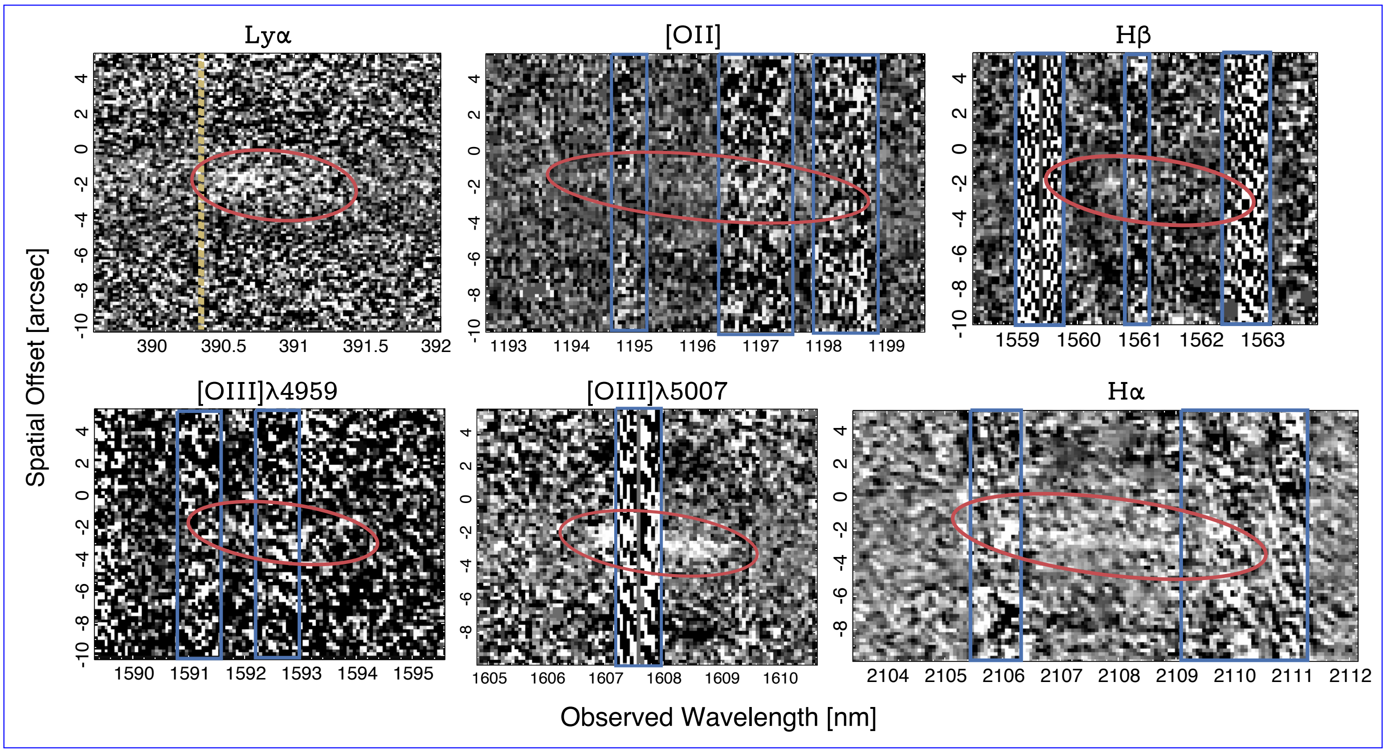

Fig. 2. 2D-images of the **emission lines corresponding to** Lyα, [O II]λ**3727,** Hβ, [O III]λ**4959,** [O III]λ5007**, and** Hα. The location of bright **skylines are** marked by blue **boxes**. The **locations** of the emission **lines are** indicated with red **ellipses**. Because the host is observed in nodding-mode, negative images of the emission **lines** appear on both sides in the spatial direction. **For the upper, left panel containing** Lyα**, the systemic redshift position of** Lyα **is marked by a yellow, vertical, dashed line. The red part of the** [O II]λ**3727-doublet is affected by atmospheric absorption.**

parameters provided by Planck Collaboration et al. (2016) in which the universe is flat with H_0 = 67.7 km s^{-1} **Mpc**$^{-1}$ **and** Ω_m = 0.307. All magnitudes are given in the AB system.

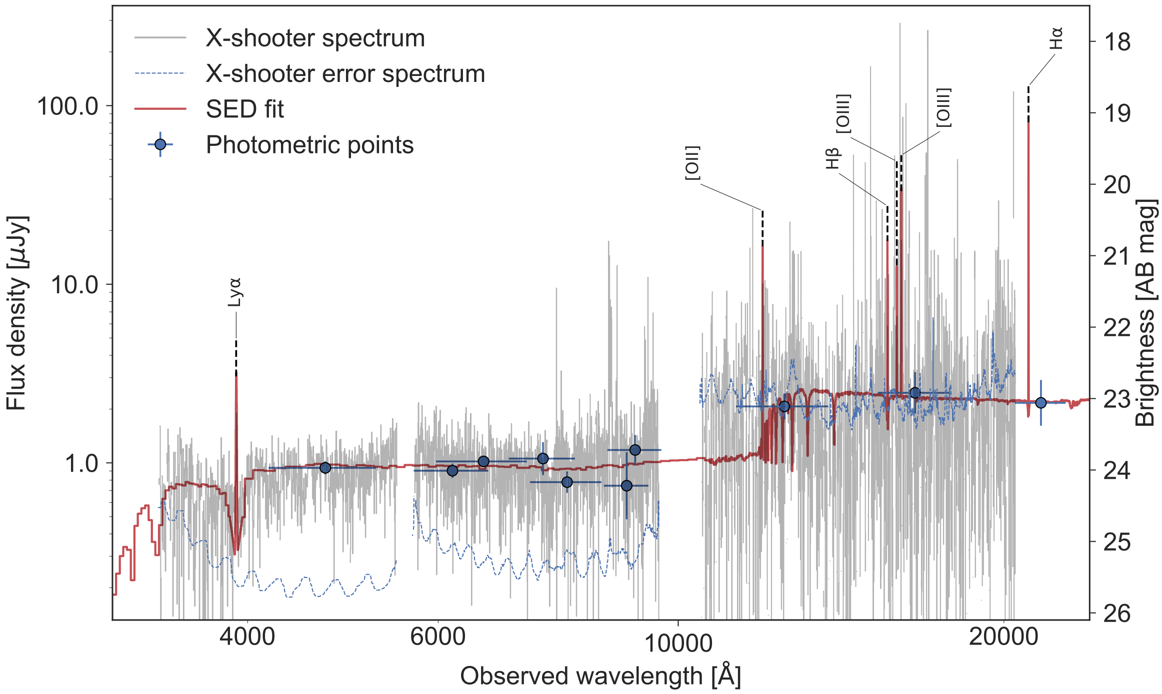

Fig. 3. Best-fit SED to the derived photometry. The detection of Lyα is predicted from the SED fit and confirmed by the spectroscopic observations. Overplotted in grey is the observed spectrum**, binned by 6 Å for presentation purposes**. **Slit losses has been corrected for based on the average seeing of the observations, as confirmed by the comparison with the photometry.** The **blue, dashed line is the corresponding error spectrum, smoothed for presentation purposes. The** reason for the spectral gaps at 5500 **Å** and 10000 **Å** is from the merging of the arms.

2. Observations and results

2.1. Spectroscopic observations and analysis

Spectroscopic observations were carried out using the cross-dispersed echelle spectrograph, VLT/X-shooter (Vernet et al. 2011), at four seperate epochs. The burst was observed 38 hours after the Burst Alert Telescope (BAT) trigger under ESO programme 088.A-0051 (PI: Fynbo) and again later under ESO programme 091.D-0904 (PI: Hjorth). Observations use a simple ABBA nodding pattern, **with** 5 ″ nod throws. X-shooter covers the wavelength range from 3000 **Å** to 24 800 **Å** (21 000 **Å** when the *K*-band blocking filter is used) across three spectroscopic arms. We carried out the bias-correction, flat-fielding, order tracing, wavelength calibration, rectification, and flux calibration using the VLT/X-shooter pipeline version 2.8.4 **(Goldoni et al. 2006, Modigliani et al. 2010)** run in physical mode. Because the echelle orders are curved across each detector, a rectification algorithm is employed which introduces correlations between neighboring pixels. We select a pixel-scale of 0.2/0.2/0.6 Å/pix for the UVB/VIS/NIR arm to minimize the degree of correlation while conserving the maximal resolution. The observations are combined and extracted using scripts described in Selsing et al. 2017 (in prep.) and available online[1]**, where the full spectral point spread function is modeled across each arm and used for** the optimal extraction algorithm (Horne 1986). An overview of the spectroscopic observations is given in Table 1, and the

[1] https://github.com/jselsing/XSGRB_reduction_scripts

slit position is shown in Fig. 1. **Each of the epochs are extracted individually and combined in a weighted fashion where the weight at each pixel is chosen as median variance spectrum of the region surrounding that pixel, thus avoiding to base the weight on the pixel variance. Slit-loss correction has been applied on the combined spectrum based on the average seeing of the observations.** We show the extracted spectrum in Fig. 3.

Table 1. Overview of the spectroscopic observations. "JH" in the slit width refers to observations where a K-band blocking filter has been used. The seeing is determined from the width of the spectral trace of a telluric standard star, observed close in time to the host observation. The spectral resolution, R, is measured from unresolved telluric absorption lines in the spectrum of the telluric standard star.

Observation epoch	Exposure time (s)			Slit width	Airmass	Seeing	R
(UT)	UVB	VIS	NIR	(arcsec)		(arcsec)	VIS/NIR
2011-11-19 01:33	2×2400	2×2400	8×600	1.0/1.0/0.9	1.49	0.75	11600/6700
2013-07-15 09:02	2×1200	2×1200	8×300	1.0/1.0/0.9JH	1.53	0.98	9600/8900
2013-08-03 07:37	2×1200	2×1200	8×300	1.0/1.0/0.9JH	1.55	0.85	11400/11300
2013-08-03 08:34	2×1200	2×1200	8×300	1.0/1.0/0.9JH	1.49	0.85	11400/11300

We determine a redshift of $z = 2.211 \pm 0.001$ from the simultaneous detection of emission lines belonging to Lyα, [O II]λ3727, Hβ, [O III]λ**4959,** [O III]λ5007, and Hα. [O II]λ**3727,** Hβ**, and** [O III]λ**4959 are** detected at low significance (∼ **3-σ). The uncertainty on the redshift is the standard deviation of independent measurements of the redshift based on the individual line centroids (excluding** Lyα**). We show cutouts of the 2D spectrum at the position of all the detected lines** in Fig. 2. Hα is only visible in the first epoch due to the K-band blocking filter used for the remaining observations. The nebular lines exhibit a spatial extent of ∼ 1$''$.5 and show significant velocity structure along the slit. A drop in the continuum bluewards of the Lyα line further supports the **redshift. No spectral evolution is observed across the epochs indicating that there is negligible GRB afterglow contribution to the first epoch spectrum.**

Using the luminosity of Hα, we can infer the **SFR** of the host (Kennicutt 1998). At the redshift of the GRB host, Hα is observed at **around** 21 000 **Å** where the night sky is very bright. In addition, several bright sky-lines are superposed on the line, making an accurate estimate of the Hα **flux difficult. Due to their velocity structure, the lines exhibit clear deviations from a Gaussian and given the low S/N of the spectra we do not attempt any parametric fits. We instead** obtain a limit on the SFR by numerically integrating the part of Hα free of contamination and **obtain** $F_{\mathrm{H,X}\alpha} > 4.1 \times 10^{-17}$ erg s^{-1} cm^{-2}. After converting the Kennicutt (1998) relation to a Chabrier (2003) initial mass function using **the conversion factor from** Madau & Dickinson (2014), we derive a limit of SFR $> 7 M_\odot$ yr^{-1}. **We additionally obtain the** Lyα **line flux by numerically integrating the entire** Lyα **line complex and obtain** $F_{\mathrm{Ly}\alpha} = (2.0 \pm 0.5) \times 10^{-17}$ erg s^{-1} cm^{-2}**, where the error on the flux is found by integrating the associated error spectrum over the same spectral region.**

From the SED-fit (Sect. 2.2) **the** host is constrained to contain very little or no dust**. Consistently,** Lyα **is detected although its presence** does not exclude dust. Therefore we do not apply a dust-correction to the measured Hα flux here. [O II] is close to a region of strong telluric absorption, which is why no SFR is inferred from this line.

The total extent of the lines in velocity space is $\sim$ 450 km $\mathbf{s}^{-1}$. The line profiles shows an asymmetric "double-horned" profile, indicating that we are seeing a galaxy with a large degree of coherent rotational motion relative to the line-of-sight. If we assume that we are viewing a spiral galaxy edge-on, this is a measure of the rotational velocity of the gas. If we assume that the spectral resolution and the turbulent width of the lines are negligible compared to the rotational velocity, we can, based on the projected size of the source and the width of the lines, put a constraint on the dynamical mass of the galaxy (de Blok & Walter 2014). Based on the physical size along the slit and the velocity width of [O III]λ5007, we infer $M_{\mathbf{dyn}} \gtrsim 10^{10.8}\ M_{\odot}$. Because we are viewing the host inclined at an angle relative to edge-on and because the slit is not aligned along the long axis of the host, this value is **a lower** limit.

2.2. Imaging observations and SED analysis

In addition to the spectroscopy presented above, we imaged the field of GRB 111117A in multiple broad-band filters using the VLT equipped with FORS2 ($gRIz$ filters) and HAWK-I (JHK_s filters). These new data are complemented by a re-analysis of some of the imaging used in Margutti et al. (2012) and Sakamoto et al. (2013) that are available to us (GTC gri-band, TNG R-band, and Gemini z-band). A log of the photometric observations and measured brightnesses is given in Table 2. **Most data were taken long after the GRB had faded when no afterglow contribution was present. Given the faintness of the afterglow (see Sect. 2.3, and Cucchiara & Cenko 2011, Cenko & Cucchiara 2011), we also expect negligible contribution to the earliest epochs, which is confirmed by the consistency between the two g-band measurements**.

All data were reduced, analyzed and fitted in a similar manner as described in detail in Krühler et al. (2011) and, more recently, in Schulze et al. (2016). **We** use our own `Python` and IRAF routines to perform a standard reduction which includes bias/flat-field correction, de-fringing (**where** necessary), sky-subtraction, and stacking of individual images. **On the final reduced image products, `DAOPHOT` (Stetson 1987) was used to derive the reported photometry, where the size of the aperture was chosen to be 2.″0. Because image quality ranges from 0.″6 - 1.″7 and the galaxy major axis is ∼ 1.″, this ensures that, in all cases, the large majority of the flux is collected and low-surface brightness light missed in the aperture will not influence the measurement. This method sacrifices some S/N in the best seeing cases for more reliable photometry across differing observing conditions.**

Photometric calibration was fixed relative to field stars from the SDSS and 2MASS catalogs in the case of $griz$ **and** JHK_s **filters, respectively**. For the R**-** and I-band photometry, we used the color transformations of Lupton[2]. We convert all magnitudes into the AB system, and correct for a Galactic foreground of E_{B-V} = 0.027 mag (Schlegel et al. 1998, Schlafly & Finkbeiner 2011).

[2] http://www.sdss3.org/dr8/algorithms/sdssUBVRITransform.php

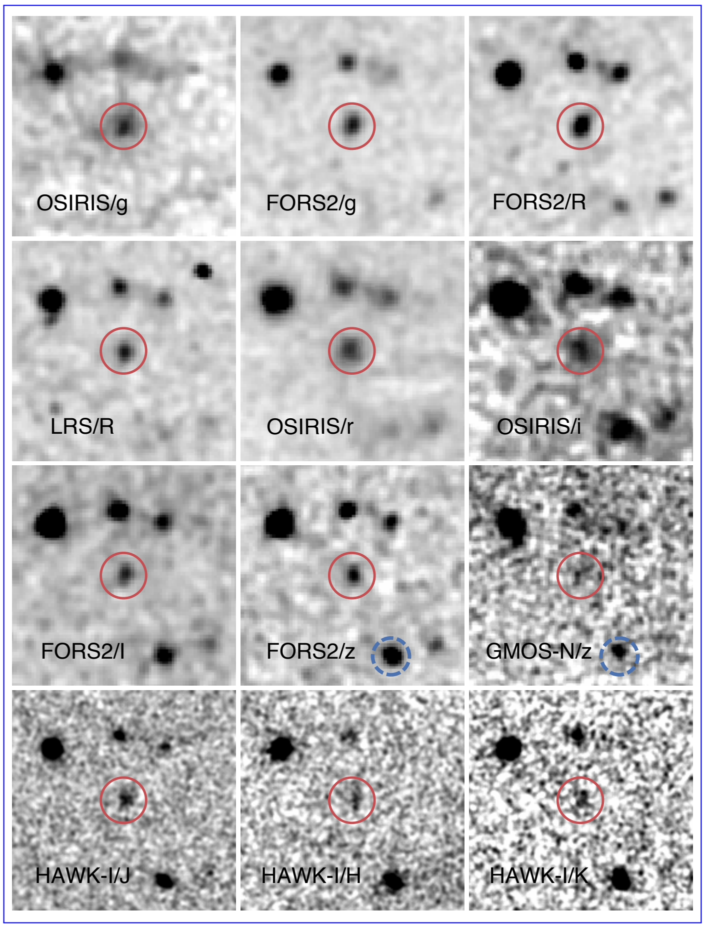

Fig. 4. Mosaic showing all used imaging. The host of GRB 111117A is marked by a red circle with a 2.″0 radius. This is the same size as the aperture used for deriving the photometry. Each panel is 20″ in size, north is up, east is left. Worth noting is the relative depth of the GMOS-N and FORS2 z-band images. For reference, the object located to the south-east of the host and marked with a blue, dashed circle has an extinction corrected magnitude of 23.11 ± 0.09 (23.10 ± 0.18) **in the FORS2 (GMOS-N) z-band.**

Noteworthy is the discrepancy of both our new VLT/FORS2 photometry and the re-analysis of the Gemini data compared to the z-band measurements of Margutti et al. (2012) and Sakamoto et al. (2013). Both of these authors report $z \sim 23$**, which is brighter than our measurement by** ~ 1.0 **mag, while data taken in other filters are consistent within the errors. Visual inspection of the Gemini image shows only a marginal detection of the host, which we report here as a $\sim$ 2-σ measurement. More conservatively, the 3-σ upper limit for the Gemini image is** $z > 24.06$**. Objects of magnitude** $z \sim 23$ **are clearly seen and are significantly brighter than the GRB host galaxy. The consistency between the deeper FORS2 z-band image and the upper limit derived for the Gemini image lends credence to the inferred magnitudes presented here, see Fig. 4.**

The multi-color SED is fit using the Bruzual & Charlot (2003) single stellar population models **(SSPs)** based on a Chabrier (2003) with initial mass function in *LePhare* (Ilbert et al. 2006), where the redshift is fixed to the spectroscopic value of $z = 2.211$. **For the SED fitting, we create a grid consisting of** $\sim 10^6$ **different galaxy templates with four metallicities 0.02, 0.2, 0.4, 1.0** $Z_{\odot}$**, different ages, star-formation histories and degrees of extinction. For every model, we calculate the likelihood, and create a probability density function (PDF) for a given parameter**

Table 2. Overview of the photometric observations.

Observation epoch (UT)	Exptime (ks)	Telescope/instrument	Filter	Airmass	Image quality (arcsec)	Host brightness[a] (AB mag)
2013-08-30 07:43	1.45	VLT/FORS2	g	1.55	0.99	24.08 ± 0.09
2011-11-17 20:07	0.80	GTC/OSIRIS	g	1.15	1.67	24.13 ± 0.09
2011-11-17 20:07	1.20	GTC/OSIRIS	r	1.11	1.50	23.93 ± 0.08
2013-07-17 08:37	1.45	VLT/FORS2	R	1.56	0.74	23.95 ± 0.06
2011-11-28 21:10	3.60	TNG/DOLORES	R	1.01	1.08	23.96 ± 0.13
2011-11-17 20:07	0.36	GTC/OSIRIS	i	1.08	1.50	23.89 ± 0.23
2013-08-03 09:23	1.35	VLT/FORS2	I	1.54	0.93	24.22 ± 0.15
2011-11-28 06:14	1.80	Gemini/GMOS-N	z	1.01	0.84	24.24 ± 0.47
2013-07-13 09:33	1.08	VLT/FORS2	z	1.49	0.63	23.76 ± 0.21
2013-06-24 09:14	1.98	VLT/HAWK-I	J	1.70	0.63	23.13 ± 0.18
2013-06-27 09:21	1.68	VLT/HAWK-I	H	1.63	0.91	22.94 ± 0.29
2013-06-28 09:14	1.92	VLT/HAWK-I	K_s	1.65	0.76	23.07 ± 0.32

Notes. [(a)] All magnitudes are given in the AB system and are not corrected for the expected Galactic foreground extinction corresponding to a reddening of $E_{B-V} = 0.027$ mag.

by marginalizing over the other parameters. We quote the median of the PDF as the best fit parameters and the errors are the 16th and 84th percentiles of the PDFs (e.g. see Schulze et al. 2016, for details on the SED fitting procedure).

The best fit model is an unreddened galaxy template**. The inferred physical parameters are the** absolute magnitude ($M_B = -22.0 \pm 0.1$ mag), **the** stellar mass ($\log(M_\star/M_\odot) = 9.9 \pm 0.2$), **the** stellar population age ($\tau = 0.5^{+0.5}_{-0.3}$ Gyr)**, and the** star-formation rate ($\mathrm{SFR_{SED}} = 11^{+9}_{-4}\ M_\odot\ \mathrm{yr}^{-1}$). We show the SED fit in Fig. 3.

Without fixing the redshift to the spectroscopic value, using the revised photometry from Table 2, the photometric redshift of the galaxy is $z_{\mathrm{phot}} = 2.04^{+0.19}_{-0.21}$, consistent with the spectroscopic value at the **1-σ** confidence level. **The large $i - z$ color found in previous works was mistakenly interpreted as the 4000 Å break, driving the galaxy photometric redshift to a lower, erroneous value.**

2.3. X-ray temporal and spectral analysis

We retrieved the automated data products provided by the *Swift*-XRT GRB repository[3] (Evans et al. 2009). The X-ray afterglow light curve can be fit with a single power-law decay with an index $\alpha = 1.27^{+0.12}_{-0.10}$. We performed a time-integrated spectral analysis using data obtained in photon counting (PC) mode in the widest time epoch where the $0.3 - 1.5$ keV to $1.5 - 10$ keV hardness ratio is constant (namely, from $t - T_0 = 205$ s to $t - T_0 = 203.5$ ks, for a total of 29.1 ks of data) to prevent spectral changes that can affect the X-ray column density determination (Kopač et al. 2012). The obtained spectrum is well described by an absorbed power-law model and the best-fit spectral parameters are a photon index of 2.1 ± 0.4 and an intrinsic equivalent hydrogen column density $N_{\mathrm{H,X}}$ of $2.4^{+2.4}_{-1.6} \times 10^{22}$ cm^{-2} ($z = 2.211$), assuming a solar abundance and a Galactic $N_{\mathrm{H,X}}$ in the burst direction of 4.1×10^{20} cm^{-2} (Willingale et al. 2013).

[3] http://www.swift.ac.uk/xrt_products/00507901

A measure of the optical-to-X-ray flux ratio is parametrized in terms of the "darkness"-parameter β_{OX} **(Jakobsson et al. 2004). Using the optical afterglow limits (**$r' > 25.5$**, 13.5 hr after the burst; Cucchiara & Cenko 2011, Cenko & Cucchiara 2011, the X-ray lightcurve can be interpolated and evaluated at the time of the non-detection. We find** $\beta_{OX} < 0.79$**, consistent with what was reported in Sakamoto et al. (2013).**

3. Reinterpretation of the rest-frame properties

Margutti et al. (2012) find a projected offset between the host nucleus and the GRB site of $1''.25 \pm 0''.20$ **arcsec; Sakamoto et al. (2013) find a similar value of** $1''.0 \pm 0''.20$ **arcsec. These correspond to a projected physical offset at** $z = 2.221$ **of** 10.6 ± 1.7 **kpc and** 8.5 ± 1.7 **kpc respectively. Because the angular** distance does not change significantly between $z = 1.3$ and $z = 2.211$, all conclusions of Margutti et al. (2012) and Sakamoto et al. (2013) relating to host offset are unaffected.

3.1. Classification

Based on the BAT light-curve, $T_{90} = 0.46$ **s which is shorter than both the prototypical 2 s (Kouveliotou et al. 1993) and the** < 0.8 **s suggested to also exclude the shorter tail of the *Swift*-observed lGRB population (Bromberg et al. 2012). Additionally, no signs of extended emission was found by Sakamoto et al. (2013). The spectral lag is** 0.6 ± 2.4 **ms, consistent with zero. As already** pointed out by Margutti et al. (2012) and Sakamoto et al. (2013), **this is typical of sGRBs, (however see also Bernardini et al. 2015). In conjunction with the duration and the spectral hardness (Sakamoto et al. 2011),** GRB 111117A is **thus** securely classified as a sGRB. Because the observed classification indicators, T_{90} and hardness ratio, do not depend strongly on redshift (Littlejohns et al. 2013), the updated redshift does not change this designation.

The intrinsic luminosity is shown in the X-ray light curve (Fig. 5) and it is sub-luminous compared to the majority of **lGRBs**. The inset in Fig. 5 shows the luminosity distribution at 10 ks. The sub-samples comprise of **402 lGRBs, 31 sGRBs**, and GRB 111117A. The **sample of lGRBs is from Evans et al. (2007, 2009) and the sample of sGRBs is compiled from Kann et al. (2011), Berger (2014) and D'Avanzo et al. (2014). The** mean and the 1-σ dispersions of the samples are $\log(L_{\mathrm{lGRB}}/\mathrm{erg\ s^{-1}}) = 46.59 \pm 0.87$ **and** $\log(L_{\mathrm{sGRB}}/\mathrm{erg\ s^{-1}}) = 44.96 \pm 0.94$ **for the lGRB and sGRB samples respectively**. GRB 111117A had $\log(L/\mathrm{erg\ s^{-1}}) = 44.95$ at 10 ks**. This** is very close to the peak of the sGRB luminosity distribution at 10 ks, but an outlier from the **lGRB** distribution, further supporting the short classification.

The separation of GRBs in two distinct classes based on their high-energy observables points to an intrinsically different physical origin. LGRBs are typically interpreted as collapsars (MacFadyen & Woosley 1999) in which a single, massive star undergoes gravitational collapse, where the currently preferred model for sGRBs is the merger of two NSs (Eichler et al. 1989, Nakar 2007). Bromberg et al. (2013) investigated the degree to which **high-energy**

observables of the long and short **GRB populations** overlap and quantified the certainty in class membership. According to Bromberg et al. (2013), GRB 111117A has **a** 96^{+3}_{-5} percent probability of being a sGRB. Compared to **two other** sGRB candidates at high redshift, GRB 060121 ($T_{90} = 1.97 \pm 0.06$ **s; de Ugarte Postigo et al. 2006, Levan et al. 2006**) at $1.7 \lesssim z \lesssim 4.5$ (17^{+14}_{-15} per cent) and GRB 090426 ($T_{90} = 1.28 \pm 0.09$ **s; Antonelli et al. 2009, Levesque et al. 2010, Thöne et al. 2011**) at $z = 2.609$ (10^{+15}_{-10} per cent), the certainty in class membership for GRB 111117A is much higher.

Additionally, Horváth et al. (2010) **classify** both GRB 060121 and GRB 090426 as **intermediate-duration** bursts. This comes from both events having very soft spectra, as compared to the hard ones typically seen in sGRBs. Intermediate bursts are very clearly related in their properties to lGRBs (de Ugarte Postigo et al. 2011), so they are unlikely to come from compact object mergers. **GRB 111117A is also securely classified as a sGRB according to the Horváth et al. (2010) classification scheme.**

A number of other GRBs are claimed to be short and at relatively high ($z \gtrsim 0.9$) redshift. If we consider bursts with a probability of being short $f_{\rm NC} > 50$ per cent, according to the Bromberg et al. (2013) classification scheme, 5 sGRB are found: GRB 051210 at $z \sim 1.3$ ($f_{\rm NC} = 82^{+10}_{-61}$ per cent; Leibler & Berger 2010), GRB 060801 at $z = 1.131$ ($f_{\rm NC} = 95^{+3}_{-5}$ per cent; Berger et al. 2007), GRB 070714 at $z = 0.923$ (no $f_{\rm NC}$ due to extended emission; Graham et al. 2009), GRB 090510 at $z = 0.903$ ($f_{\rm NC} = 97^{+1}_{-29}$ per cent; McBreen et al. 2010), and GRB 100117 at $z = 0.915$ ($f_{\rm NC} = 97^{+1}_{-3}$ per cent; Fong et al. 2011). Although in individual cases a secure host association (hence redshift determination) is uncertain, there does seem to be a number of sGRBs at $z \sim 1$.

This securely makes GRB 111117A, by far, the highest redshift sGRB detected to date. The redshift and classification of GRB 111117A **imply** that it occurred when the universe was younger by ∼ **3** Gyr compared to any other **securely classified sGRB** ever detected. If the merger of NSs is the primary agent for the *r*-process element enrichment of the universe (Goriely et al. 2011, Ji et al. 2016, Komiya & Shigeyama 2016), this marks the earliest detection of this process.

3.2. Rest-frame $N_{\rm H,X}$

We show the recalculated **hydrogen equivalent X-ray derived column density,** $N_{\rm H,X}$**,** in Fig. 6 where we compare with the distributions of complete samples of both long and short GRBs. The lGRB sample is from Arcodia et al. (2016) and the sGRB sample is from D'Avanzo et al. (2014). From the sGRB sample of D'Avanzo et al. (2014) we have excluded GRB 090426 which does likely not belong in a short sample as highlighted in Sect. 3.1. Both comparison samples **infer** $N_{\rm H,X}$ **over** the largest temporal interval of constant hardness ratio to **exclude** spectral changes that can affect the X-ray derived column density. The 17 (5) of the 99 (15) long (short) GRBs which do not have **measured redshifts** have been excluded from our analysis.

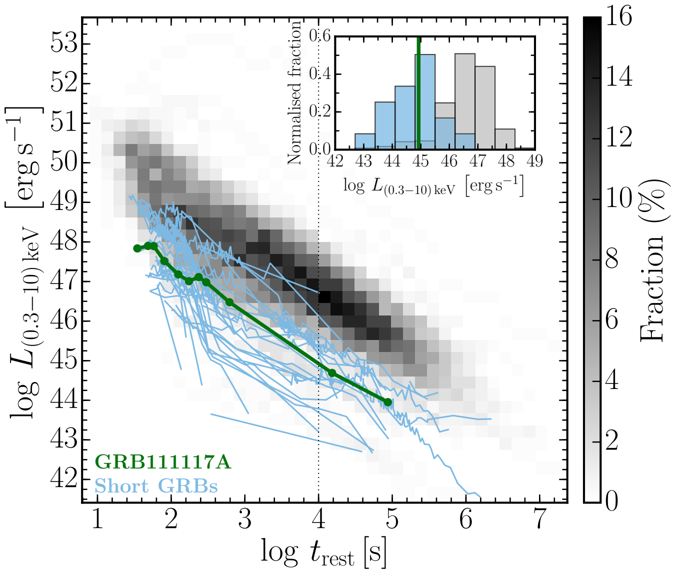

Fig. 5. Rest-frame XRT lightcurve of GRB 111117A, compared to the general population of XRT lightcurves of GRBs. The grey shaded region is a compilation of long GRB lightcurves (Evans et al. 2007, 2009) where the color represents density. The light blue lines are sGRB lightcurves from bursts with duration of $T_{90} \lesssim 2$ s and those that were classified as short in Kann et al. (2011), Berger (2014), D'Avanzo et al. (2014). The thick green line is GRB 111117A. Despite the remarkably high redshift, the luminosity is comparable to the bulk of the short burst population and subluminous compared to the lGRB population. **The insert shows the X-ray luminosity distributions of sGRBs and lGRBs at 10 ks, indicated by the vertical dashed line in the main panel.**

GRB 111117A occupies a unique position in Fig. 6 with the highest $N_{\mathrm{H,X}}$ and highest redshift of all sGRBs. The short sample, excluding GRB 111117A, is located at low **redshift** ($z < 1$) and is found to populate a column density environment similar to that of lGRBs at comparable redshifts (D'Avanzo et al. 2014). The inferred hydrogen column density for GRB 111117A seems to follow the trend with increasing $N_{\mathrm{H,X}}$ as a function of redshift as found for the lGRB afterglows (Campana et al. 2010, Starling et al. 2013, Arcodia et al. 2016). This is related to what is found by Kopač et al. (2012), Margutti et al. (2013), that $N_{\mathrm{H,X}}$ seems to be comparable for long and short GRBs when compared at similar redshifts.

The redshift evolution of $N_{\mathrm{H,X}}$ in the hosts of lGRBs is not reproduced by Buchner et al. (2017), using a different $N_{\mathrm{H,X}}$ inference methodology. Instead a correlation between $N_{\mathrm{H,X}}$ and host stellar mass is suggested. Assuming that the different $N_{\mathrm{H,X}}$-fitting methodologies yield comparable results, GRB 111117A **has a larger** $N_{\mathrm{H,X}}$ **compared to** the relation suggested by Buchner et al. (2017) by more than the intrinsic scatter, although some lGRB hosts populate a similar region in the $N_{\mathrm{H,X}}$-$M_{\star}$ relation.

The large offset of GRB 111117A relative to the host center derived in Margutti et al. (2012) and Sakamoto et al. (2013) is difficult to reconcile with galaxy-scale gas being the source of the X-ray absorption. Along with the low dust content of the host, the large offset from the host center indicates that the high $N_{\mathrm{H,X}}$ arises because the density in the GRB surroundings is high, or because the light from the afterglow transverses localized regions of dense gas, similar to what is found by (). Alternatively, a significant contribution to the observed X-ray $N_{\mathrm{H,X}}$ can come from the diffuse intergalactic medium and the intervening

systems along the line of sight of the GRB (Campana et al. 2012, Arcodia et al. 2016), although see ()

The large offset of GRB 111117A relative to the host center derived in Margutti et al. (2012) and Sakamoto et al. (2013) is difficult to reconcile with galaxy-scale gas **being the source of the** X-ray absorption. Along with the **low dust content of the host**, the large offset from the host center indicates that the high $N_{\rm H,X}$ arises because the density in the GRB **surroundings is high (or possibly** because the light from the afterglow **transverses localized regions** of dense gas**), see for example, (e.g. Watson et al. 2013, Krongold & Prochaska 2013). Alternatively, it has been hypothesised that a significant contribution to the observed X-ray $N_{\rm H,X}$ could come from the diffuse intergalactic medium and the intervening systems along the line of sight of the GRB (Campana et al. 2012, Arcodia et al. 2016), although see (Watson et al. 2013, Krongold & Prochaska 2013).**

Even assuming a low dust-to-metals ratio as typically observed in long GRB afterglow sightlines (Galama & Wijers 2001, Schady et al. 2010, Covino et al. 2013), the $N_{\rm H,X}$ value derived from the X-ray spectrum corresponds to significant extinction along the afterglow line of sight ($A_V \gtrsim 1$ mag), which is contrasted to the absence of dust found from the SED fit and supported by the detection of Lyα. Such a discrepancy between the extinction derived from the GRB afterglow and the one obtained using galaxy-wide measures has also been observed occasionally for lGRBs (Perley et al. 2013). For the one sGRB where both parameters were measured (GRB 130603B; de Ugarte Postigo et al. 2014), they were found to be consistent with $A_V \sim 1$ mag.

The lack of optical detection is also consistent with a high column along the GRB line of sight, as dust extinction could contribute to the optical faintness. On the contrary, its X-ray afterglow flux lies within the expected distribution given its gamma-ray fluence (D'Avanzo et al. 2014). This is not unexpected, as the X-ray flux is independent of the surrounding medium density (Freedman & Waxman 2001, Berger et al. 2003, Nysewander et al. 2009).

3.3. Host galaxy

Because of the secure host association, GRB 111117A does not belong to the hostless class of **sGRBs** (Berger 2010) and because the host exhibits emission lines this is indicative of a population of relatively young stars. **Like** the majority of sGRBs (Fong et al. 2013), the host of GRB 111117A is therefore a late-type galaxy and is entirely consistent in terms of stellar mass and stellar age with the general population of sGRB hosts ($\langle M_* \rangle = 10^{10.1} M_\odot$ and $\langle \tau_* \rangle = 0.3$ Gyr; **Leibler & Berger 2010**). Being a late-type host, both the stellar mass and sSFR are entirely within the range expected for the hosts of sGRBs (Behroozi et al. 2014). Our **constraint** on the dynamical mass is also well accommodated by the expected sGRB host halo mass (Behroozi et al. 2014).

The SFR is ~1 order of magnitude higher than the typical SFR for sGRB host galaxies (Berger 2014) and more similar to the SFR found in the hosts of lGRBs at a corresponding redshift (Krühler

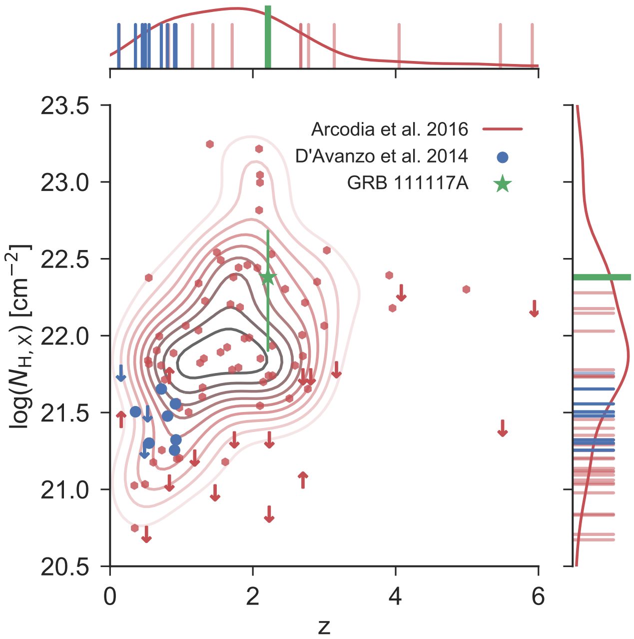

Fig. 6. Rest frame, X-ray derived equivalent hydrogen column **density of** GRB 111117A compared to complete samples of both long and short populations of GRBs. The **sample of lGRBs from Arcodia et al. (2016) is shown in red, where** detections are **also shown** with **a kernel density estimate of the points** and the limits **on** $N_{H,X}$ are shown with arrows. **The complete sample of sGRB by D'Avanzo et al. (2014) is shown in blue, where again the limits are indicated by arrows. Marginalizations over both axes are shown on the right and on the top of the plot, where the limits are shown as semi-transparent bars and detections as solid ones. The red curves in the marginalization plots are again the kernel density estimates of the Arcodia et al. (2016) sample.**

et al. 2015). Only two hosts in the sample of short GRBs compiled **by** Berger (2014) have a more vigorous star formation, **placing** it is in the very upper end of the star formation distribution. The cosmic SFR evolution of the universe likely plays a role due to the proximity of GRB 111117A to the peak of cosmic SFR (Madau & Dickinson 2014). The high SFR is partly a selection effect, because a less star forming galaxy would exhibit weaker emission lines, thus making the redshift harder to determine. Additionally, it is natural to expect some evolution in the hosts of sGRBs with redshift as illustrated for $N_{H,X}$ in Sect. 3.2.

The **simultaneus detection of** Lyα **and** Hα **allows us to put constraints of the escape fraction of** Lyα, f_{esc}(Lyα)**. Using the intrinsic ratio between** Hα **and** Lyα**, assuming case B recombination (Brocklehurst 1971), and the measured fluxes from the spectrum, we find** f_{esc}(Lyα)< 0.06**. While the** f_{esc}(Lyα) **scales with the dust column (Hayes et al. 2011), the resonant scattering of** Lyα**-photons with neutral hydrogen makes the effective path length of** Lyα **longer than for** Hα **(Atek et al. 2009). This makes** f_{esc}(Lyα) **an unreliable proxy for dust column, especially at low dust columns (Atek et al. 2014) where the geometry and dynamics of the** H I **within the galaxy will affect the** Lyα **path the most. The** f_{esc}(Lyα) **inferred for the host is entirely consistent with what is found for field galaxies with similar properties (Oyarzún et al. 2017). The same authors also find that** Lyα **emitting galaxies have mostly little dust, consistent with what inferred from the SED fit(see Sect. 2.2). The** centroid of the Lyα emission is found to be redshifted by $\sim 240 \pm 90$ km s^{-1} with respect to systemic, which is similar to what is found for long GRB hosts (Milvang-Jensen et al. 2012) **and Lyman break galaxies (Shapley et al. 2003) in which** the outflow is attributed to star formation.

4. Implications for the redshift distribution of sGRBs

The redshift distribution of GRBs is a powerful informant on both the conditions which drive the formation of these events, but also on the potential influence these cosmic explosions have on the evolution of the universe. Due to the elevated brightness of lGRBs compared to sGRBs (Berger 2014) and their tendency to be associated with the star-forming and therefore dense regions in their hosts (Fruchter et al. 2006, Lyman et al. 2017), the redshifts of lGRBs are easier to measure than for sGRB counterparts, where only a single burst has a redshift measurement from the GRB afterglow (Cucchiara et al. 2013, de Ugarte Postigo et al. 2014). Correspondingly, the redshift distribution of sGRBs is still substantially unconstrained compared to that of lGRBs (e.g., see Jakobsson et al. 2012, D'Avanzo 2015, Perley et al. 2016).

A single sGRB at high redshift does little in terms of constraining the redshift distribution of sGRBs. In particular, other sGRB **host redshifts could have been missed because their hosts** are intrinsically fainter and thus the high redshift of GRB 111117A is only measured due to the brightness of its host. Berger (2014) compiled a sample of sGRB host luminosities, normalized by the characteristic galaxy luminosity at their respective redshift, $L_B/L_B^{\star}$. To convert the SED-inferred M_B of GRB 111117A to $L_B/L_B^{\star}$, we use the characteristic absolute B-band magnitude of the Schechter function for blue galaxies ($U - V < 0.25$) in the redshift window $2.0 \leq z \leq 2.5$ from Marchesini et al. (2007) and obtain $L_B/L_B^{\star} = 1.2$.

Using the complete, flux-limited selection of ***Swift*-detected** bursts from D'Avanzo et al. (2014), excluding GRB 111117A and the likely non-sGRB GRB 090426, we have a statistically homogeneous sample from which we can address the implications of the redshift of GRB 111117A. **This sample includes sGRB originating in star-forming galaxies, elliptical galaxies, and apparent hostless sGRBs.** Out of the 14 hosts in the sample, 10 (71 per cent) have **both** measured redshifts and $L_B/L_B^{\star}$. **Compared to** the complete sample, the host of GRB 111117A is brighter than 80 per cent of the hosts with measured $L_B/L_B^{\star}$. Even if we conservatively assume that *all* the hosts missing $L_B/L_B^{\star}$ are brighter than the host of GRB 111117A, the host is still brighter than > 60 per cent of sGRB hosts. For all 26 hosts with $L_B/L_B^{\star}$ from Berger (2014), the host of GRB 111117A is brighter than 73 per cent.

If we assume that we are able to obtain emission-line redshifts from hosts **which are at most** 0.5 **mag** fainter ($R < 24.5$ mag; Krühler et al. 2012), then we would have missed 60 per cent of the redshifts (6 out of 10 hosts), **due too the host being too faint,** were they at the redshift of GRB **11117A**. The corresponding number is around 45 per cent (12 out of 26) from the full sample of Berger (2014), reflecting the lower mean $L_B/L_B^{\star}$ of the complete sample. Because the average SFR of galaxies hosting lGRBs is higher than for galaxies hosting sGRBs, the fraction of missed burst redshifts is likely higher although the cosmic SFR evolution could play a role in improving redshift determinability **at high** z.

A fraction of the bursts missing redshift are host-less but appear to be spatially correlated with galaxies that are likely at moderate redshifts (Tunnicliffe et al. 2014), but should some of the remainder be at high redshift, the missed fraction will increase. If we assume that *all* the bursts that are missing redshifts are at high-z and missed due to host faintness, 10 out of 14 hosts in the complete sample (71 per cent) would be missed at $z = 2.211$. This serves as an upper limit on the fraction of missed burst redshifts at high-z. Conversely, if all bursts missing redshift are at low redshift and missed for other reasons, 6 out of 14 hosts (43 per cent) would be missed at $z = 2.211$. The two limits indicate that we would miss between 43 and 71 per cent of ***Swift*-detected** sGRB hosts at $z \sim 2$ due to host faintness.

The theoretical redshift distribution of sGRBs depends on the type of delay-time function used to model the progenitor system. The likelihood preferred lognormal time delay models investigated by Wanderman & Piran (2015) predict a sGRB rate at $z = 2.211$, **around** two orders of magnitude lower compared to the peak rate at $z = 0.9$. According to Wanderman & Piran (2015), this preference depends critically on the absence of sGRBs at $z \gtrsim 1.2$. The higher determined redshift of GRB 111117A, and the likely number of additional **high-z** sGRB could change the preferred time delay models. The redshift of GRB 111117A, on the other hand, is close to the expected peak in sGRB rate calculated using the power law delay time models **(Behroozi et al. 2014, Wanderman & Piran 2015, Ghirlanda et al. 2016), meaning we would be missing a large fraction of sGRB redshifts**.

A critical test to assess if the power law delay time models can be accommodated by the current observation is to check if the implied sGRB rate at higher redshift does not exceed the number of observed sGRBs without redshifts. Of the 100 sGRBs observed by *Swift*, 20 have secure redshifts, and another 7 have a tentative redshift measurement[4], meaning that >73 per cent of all sGRBs observed with *Swift* are missing redshifts. More recently, Fong et al. (2017) (LIGO Scientific Collaboration et al. 2017) compiled a list of 36 (33) sGRBs with redshift measurements and, using this number, the redshift incompleteness of sGRBs decreases to 64 per cent. Additional to the potential number of high-z event already detected but missing redshifts, Behroozi et al. (2014) parametrized the *Swift* redshift sensitivity and found that the mean detection probability for sGRBs at $z \sim 2$ was only ~ 1 per cent of the mean detection probability at $z \sim 1$, assuming that the unknown beaming angle of sGRBs stays constant with time. What this means is that at the present, there is almost no limit on the number of sGRBs that could be at higher redshifts.

[4] **This is based on http://www.astro.caltech.edu/grbox/grbox.php, selecting all short, *Swift*-detected GRBs up to GRB 170428A.**

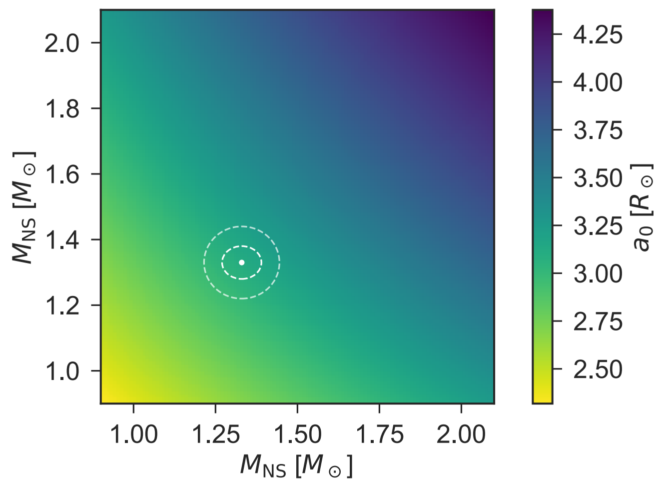

Fig. 7. Constraints on the initial progenitor separation, given binary constituent masses. As can be seen, a heavier system will inspiral faster, leading to a weaker constraint on the initial separation of the binary. The most probable value, the 68 per cent, and 98 percent posterior predictive intervals of the NS binary mass distribution from Kiziltan et al. (2013) are shown with the dashed ellipses, which corresponds to a constraint on maximal initial separation of $a_0 < 3.1^{+0.2(+0.4)}_{-0.2(-0.4)}$ $R_\odot$, respectively.

5. Constraints on progenitor separation

At $z = 2.211$, the age of the universe is 3 Gyr. If the progenitor systems of sGRBs are the merger of two NSs, this sets a hard upper limit to the coalescence timescale for such a system. In the absence of other mechanisms, the timescale of the orbital decay of the system is set by the energy loss due to **GWs**, which in turn is set by the mass of the constituent compact objects, the eccentricity of the orbit**,** and the separation of the two (Postnov & Yungelson 2014). If we assume that the formation timescale of the first galaxies is short compared to the time since the Big Bang (Richard et al. 2011), and **that any binary NS formation channel can work sufficiently fast, we can, assuming** a mass of each of the NSs in a circular orbit at the time of system formation, **place** a hard upper limit on the initial separation, a_0.

In practice most NS-NS binaries will be eccentric at formation because of the SN natal kicks. For more eccentric orbits, the coalescence timescale decreases, leading to a larger initial separation **constraint**. As noted by Postnov & Yungelson (2014), it takes eccentricities > 0.6 to significantly shorten the merger time. **Due to tidal interactions between the two NSs, the orbits will also tend to circularize with time, lessening the impact of the eccentricity on the constraint.**

Additionally, the constraint on initial progenitor separation will change depending on the mass assumed for the constituent NS masses, with larger masses generally resulting in faster inspiral times and weaker constraints of initial separation. We use the NS mass distribution from Kiziltan et al. (2013) to compute a grid of initial progenitor separation constraints, given the range of NS masses allowed. We show the grid in Fig. 7. The double NS binary systems have a constituent mass distribution peaked at $1.33^{+0.10}_{-0.12}$ $M_\odot$ (Kiziltan et al. 2013), which corresponds to $a_0 < 3.1^{+0.2}_{-0.2}$ $R_\odot$ where the errors are the 68 per cent posterior predictive intervals.

Using the inferred stellar population age from our SED fit, we obtain a **less robust** limit on the initial separation of $a_0 < 2.0^{+0.4}_{-0.4}\ R_\odot$. However, this does not account for the possibility there could be an underlying stellar population of older stars from a previous star-formation **episode. To investigate the possible impact of the presence of an old stellar population, we followed Papovich et al. (2001) and re-fitted the observed SED with the best-fit template to which an additional stellar population of old stars was added. For each template, this old population was set as the SSP with the same parameters as the best-fit SED except the age, which was set to the age of the Universe at the observed redshift. In principle, this can constrain the maximum contribution of old populations within the photometric error bars (see Papovich et al. 2001, for details). We find a negligible contribution to the stellar mass (i.e. variations much smaller than the statistical uncertainty associated with the best-fit template).**

The delay time between formation and explosion is well accommodated by the models of Belczynski et al. (2006), although the longest delay times are excluded. This is especially true given the late type nature of the host (O'Shaughnessy et al. 2008). **The same holds, if NS binaries are primarily formed through dynamical interactions in globular clusters (Lee et al. 2010, Church et al. 2011).**

6. Conclusions

We have here provided a revised, spectroscopic redshift measurement for the short GRB 111117A based on host galaxy emission lines setting it at $z = 2.211 \pm 0.001$. This value supersedes the previous photometric redshift **estimates** of Margutti et al. (2012) and Sakamoto et al. (2013). The erroneous **best-fit SED redshift** of previous authors is attributed to a discrepancy in the measured z-band magnitude, and highlights the importance of deep spectroscopic studies of sGRB hosts at medium resolution.

Using the new distance, the X-ray derived $N_{\mathrm{H,X}}$ towards GRB 111117A is the highest within a complete sample of **sGRBs** and is consistent with the $N_{\mathrm{H,X}} - z$ evolution traced by the **sight lines** of lGRBs. The SFR of the host is in the upper end of the sGRB host SFR distribution and no **significant amount of** dust is present. The high $N_{\mathrm{H,X}}$ **is at odds** with the large projected host offset and the absence of dust. One possible explanation could be that GRB 111117A is formed through a prompt channel of sGRB formation and originates in **an (unseen)** star forming region located in the outskirts of the host**, or a localized region of high** H I **density along the line of sight**.

Although a single burst carries little leverage in terms of constraining the redshift distribution of sGRB, the high redshift of GRB 111117A needs to be accommodated in progenitor models. A lognormal delay time model predicts a very low volumetric density of bursts at $z \sim 2$, whereas a power law delay time model peaks near **the** GRB 111117A **redshift**. If more sGRBs are at similarly high redshifts, but are missed due to the faintness of their hosts **and afterglows**, a lognormal delay time model will be disfavored. Compared to a **complete sample of *Swift*-detected sGRB, the host of** GRB 111117A is more luminous than 80 per cent of sGRB hosts with measured luminosities.

Assuming a host brightness redshift determination threshold, for between 43 and 71 per cent of **the sample** hosts, we would be unable to determine a redshift should they be at a similar redshift **of** GRB 111117A. This could indicate that**,** potentially, a significant fraction of ***Swift*-detected** sGRBs are at high z**, but with redshifts unknown** due to host faintness.

Using the age of the universe at the time of explosion allows us to set constraints on the maximal separation between the engine constituents at the time of formation. We find that the maximal separation of two NSs at system formation time is $a_0 < 3.1\ R_{\odot}$, which excludes some of the formation channels with the longest timescales.

All data, code and calculations related to the paper along with the paper itself are available at `https://github.com/jselsing/GRB111117A`.

Acknowledgements. We thank **the anonymous referee for a constructive report. We thank** Jens Hjorth and Lise Christensen for useful discussions regarding the interpretation of this event. **We thank Mathieu Puech for testing the possible contribution from an older stellar population in the SED. We thank Peter Laursen for fruitful discussions regarding the** Lyα **escape fraction.** TK acknowledges support through the Sofja Kovalevskaja Award to P. Schady. **SDV is supported by the French National Research Agency (ANR) under contract ANR-16-CE31-0003 BEaPro. PDA, SCo, acknowledge support from ASI grant I/004/11/3.** JJ acknowledges support from NOVA and NWO-FAPESP grant for advanced instrumentation in astronomy. NRT and KW acknowledge support from STFC Consolidated Grant ST/N000757/**1.** CT acknowledges support from a Spanish National Research Grant of Excellence under project AYA 2014-58381-P and funding associated to a Ramón y Cajál fellowship under grant number RyC-2012-09984. AdUP acknowledges support from a Ramón y Cajal fellowship, a BBVA Foundation Grant for Researchers and Cultural Creators, and the Spanish Ministry of Economy and Competitiveness through project AYA2014-58381-P. ZC acknowledges support from the Spanish research project AYA 2014-58381-P and support from Juan de la Cierva Incorporación fellowships IJCI-2014-21669. RSR acknowledges AdUP's BBVA Foundation Grant for Researchers and Cultural Creators and support from ASI (Italian Space Agency) through the Contract n. 2015-046-R.0 and from European Union Horizon 2020 Programme under the AHEAD project (grant agreement n. 654215). This research made use of Astropy, a community-developed core Python package for Astronomy (Astropy Collaboration 2013). The analysis and plotting has been achieved using the Python-based packages Matplotlib (Hunter 2007), Numpy**,** and Scipy (van der Walt et al. 2011)**,** along with other community-developed packages. This work made use of observations obtained with the Italian 3.6 m Telescopio Nazionale Galileo (TNG) operated on the island of La Palma by the Fundación Galileo Galilei of the INAF (Istituto Nazionale di Astrofisica) at the Spanish Observatorio del Roque de los Muchachos of the Instituto de Astrofísica de Canarias. Based on data from the GTC Archive at CAB (INTA-CSIC) and on observations obtained at the Gemini Observatory, which is operated by the Association of Universities for Research in Astronomy, Inc., under a cooperative agreement with the NSF on behalf of the Gemini partnership: the National Science Foundation (United States), the National Research Council (Canada), CONICYT (Chile), Ministerio de Ciencia, Tecnología e Innovación Productiva (Argentina), and Ministério da Ciência, Tecnologia e Inovação (Brazil).

References

Abbott B. P., et al., 2017a, Nature

Abbott B. P., et al., 2017b, Phys. Rev. Lett., 119, 161101

Antonelli L. A., et al., 2009, A&A, 507, L45

Arcodia R., Campana S., Salvaterra R., 2016, A&A, 590, A82

Arun K. G., Tagoshi H., Pai A., Mishra C. K., 2014, Phys. Rev. D, 90, 024060

Astropy Collaboration 2013, A&A, 558, A33

Atek H., Kunth D., Schaerer D., Hayes M., Deharveng J. M., Östlin G., Mas-Hesse J. M., 2009, A&A, 506, L1

Atek H., Kunth D., Schaerer D., Miguel Mas-Hesse J., Hayes M., Östlin G., Kneib J.-P., 2014, A&A, 561, A89

Barnes J., Kasen D., 2013, ApJ, 775, 18

Behroozi P. S., Ramirez-Ruiz E., Fryer C. L., 2014, ApJ, 792, 123

Belczynski K., Perna R., Bulik T., Kalogera V., Ivanova N., Lamb D. Q., 2006, ApJ, 648, 1110

Berger E., 2010, ApJ, 722, 1946

Berger E., 2014, ARA&A, 52, 43

Berger E., Kulkarni S., Frail D., 2003, ApJ, 590, 379

Berger E., et al., 2007, ApJ, 664, 1000

Berger E., Fong W., Chornock R., 2013, ApJ, 774, L23

Bernardini M. G., et al., 2015, MNRAS, 446, 1129

Brocklehurst M., 1971, MNRAS, 153, 471

Bromberg O., Nakar E., Piran T., Sari R., 2012, ApJ, 749, 110

Bromberg O., Nakar E., Piran T., Sari R., 2013, ApJ, 764, 179

Bruzual G., Charlot S., 2003, MNRAS, 344, 1000

Buchner J., Schulze S., Bauer F. E., 2017, MNRAS, 464, 4545

Campana S., Thöne C. C., de Ugarte Postigo A., Tagliaferri G., Moretti A., Covino S., 2010, MNRAS, 402, 2429

Campana S., et al., 2012, MNRAS, 421, 1697

Cenko S. B., Cucchiara A., 2011, GRB Coord. Network, Circ. Serv. No. 12577, 12577

Chabrier G., 2003, PASP, 115, 763

Church R. P., Levan A. J., Davies M. B., Tanvir N., 2011, MNRAS, 413, 2004

Covino S., et al., 2013, MNRAS, 432, 1231

Cucchiara A., Cenko S. B., 2011, GRB Coord. Network, Circ. Serv. No. 12567,, 12567

Cucchiara A., et al., 2013, ApJ, 777, 94

D'Avanzo P., 2015, JHEAp, 7, 73

D'Avanzo P., et al., 2014, MNRAS, 442, 2342

Della Valle M., et al., 2006, Nature, 444, 1050

Eichler D., Livio M., Piran T., Schramm D. N., 1989, Nature, 340, 126

Evans P. A., et al., 2007, A&A, 469, 379

Evans P. A., et al., 2009, MNRAS, 397, 1177

Fong W., Berger E., 2013, ApJ, 776, 18

Fong W.-f., et al., 2011, ApJ, 730, 26

Fong W., et al., 2013, ApJ, 769, 56

Fong W., et al., 2017, Astrophys. J. Lett., 848, L23

Fox D. B., et al., 2005, Nature, 437, 845

Freedman D. L., Waxman E., 2001, ApJ, 547, 922

Fruchter A. S., et al., 2006, Nature, 441, 463

Fynbo J. P. U., et al., 2006, Nature, 444, 1047

Gal-Yam A., et al., 2006, Nature, 444, 1053

Galama T. J., Wijers R. A. M. J., 2001, ApJ, 549, L209

Gehrels N., et al., 2004, ApJ, 611, 1005

Ghirlanda G., et al., 2016, A&A, 594, A84

Goldoni P., Royer F., François P., Horrobin M., Blanc G., Vernet J., Modigliani A., Larsen J., 2006, Ground-based Airborne Instrum. Astron. Ed. by McLean, 6269, 80

Goldstein A., et al., 2017, Astrophys. J. Lett., 848, L14

Goriely S., Bauswein A., Janka H.-T., 2011, ApJ, 738, L32

Graham J. F., et al., 2009, ApJ, 698, 1620

Hayes M., Schaerer D., Östlin G., Mas-Hesse J. M., Atek H., Kunth D., 2011, ApJ, 730, 8

Hjorth J., et al., 2005a, Nature, 437, 859

Hjorth J., et al., 2005b, ApJ, 630, L117

Horne K., 1986, PASP, 98, 609

Horváth I., Bagoly Z., Balázs L. G., de Ugarte Postigo A., Veres P., Mészáros A., 2010, ApJ, 713, 552

Hunter J. D., 2007, CSE, 9, 90

Ilbert O., et al., 2006, A&A, 457, 841

Jakobsson P., Hjorth J., Fynbo J. P. U., Watson D., Pedersen K., Björnsson G., Gorosabel J., 2004, ApJ, 617, L21

Jakobsson P., et al., 2012, ApJ, 752, 62

Ji A. P., Frebel A., Chiti A., Simon J. D., 2016, Nature, 531, 610

Jin Z.-P., et al., 2016, Nat. Commun., 7, 12898

Kann D. A., et al., 2011, ApJ, 734, 96

Kennicutt R. C., 1998, ARA&A, 36, 189

Kiziltan B., Kottas A., De Yoreo M., Thorsett S. E., 2013, ApJ, 778, 66

Komiya Y., Shigeyama T., 2016, ApJ, 830, 76

Kopač D., et al., 2012, MNRAS, 424, 2392

Kouveliotou C., Meegan C. A., Fishman G. J., Bhat N. P., Briggs M. S., Koshut T. M., Paciesas W. S., Pendleton G. N., 1993, ApJ, 413, L101

Krongold Y., Prochaska J. X., 2013, ApJ, 774, 115

Krühler T., et al., 2011, A&A, 526, A153

Krühler T., et al., 2012, ApJ, 758, 46

Krühler T., et al., 2015, A&A, 581, A125

LIGO Scientific Collaboration Virgo Collaboration Monitor F. G.-R. B., INTEGRAL 2017, ApJ, 848, L13

Lee W. H., Ramirez-Ruiz E., van de Ven G., 2010, ApJ, 720, 953

Leibler C. N., Berger E., 2010, ApJ, 725, 1202

Levan A. J., et al., 2006, ApJ, 648, L9

Levesque E. M., et al., 2010, MNRAS, 401, 963

Littlejohns O. M., Tanvir N. R., Willingale R., Evans P. A., O'Brien P. T., Levan A. J., 2013, MNRAS, 436, 3640

Lyman J. D., et al., 2017, MNRAS, 1817, stx220

MacFadyen A. I., Woosley S. E., 1999, ApJ, 524, 262

Madau P., Dickinson M., 2014, ARA&A, 52, 415

Marchesini D., et al., 2007, ApJ, 656, 42

Margutti R., et al., 2012, ApJ, 756, 63

Margutti R., et al., 2013, MNRAS, 428, 729

McBreen S., et al., 2010, A&A, 516, A71

Milvang-Jensen B., Fynbo J. P. U., Malesani D., Hjorth J., Jakobsson P., Møller P., 2012, ApJ, 756, 25

Modigliani A., et al., 2010, SPIE Astron. Telesc. + Instrum., 7737, 773728

Nakar E., 2007, Phys. Rep., 442, 166

Nissanke S., Holz D. E., Hughes S. A., Dalal N., Sievers J. L., 2010, ApJ, 725, 496

Norris J. P., Bonnell J. T., 2006, ApJ, 643, 266

Nysewander M., Fruchter A. S., Pe'er A., 2009, ApJ, 701, 824

O'Shaughnessy R., Belczynski K., Kalogera V., 2008, ApJ, 675, 566

Oyarzún G. A., Blanc G. A., González V., Mateo M., Bailey J. I., 2017, ApJ, 843, 133

Papovich C., Dickinson M., Ferguson H. C., 2001, ApJ, 559, 620

Perley D. A., et al., 2013, ApJ, 778, 128

Perley D. A., et al., 2016, ApJ, 817, 7

Planck Collaboration et al., 2016, A&A, 594, A13

Postnov K. A., Yungelson L. R., 2014, LRR, 17

Richard J., Kneib J.-P., Ebeling H., Stark D. P., Egami E., Fiedler A. K., 2011, Mon. Not. R. Astron. Soc. Lett., 414, L31

Rosswog S., Feindt U., Korobkin O., Wu M.-R., Sollerman J., Goobar A., Martinez-Pinedo G., 2017, Class. Quantum Gravity, 34, 104001

Sakamoto T., et al., 2011, ApJS, 195, 2

Sakamoto T., et al., 2013, ApJ, 766, 41

Savchenko V., et al., 2017, Astrophys. J. Lett., 848, L15

Schady P., et al., 2010, MNRAS, 401, 2773

Schlafly E. F., Finkbeiner D. P., 2011, ApJ, 737, 103

Schlegel D. J., Finkbeiner D. P., Davis M., 1998, ApJ, 500, 525

Schulze S., et al., 2016, eprint arXiv:1612.05978

Shapley A. E., Steidel C. C., Pettini M., Adelberger K. L., 2003, ApJ, 588, 65

Starling R. L. C., Willingale R., Tanvir N. R., Scott A. E., Wiersema K., O'Brien P. T., Levan A. J., Stewart G. C., 2013, MNRAS, 431, 3159

Stetson P. B., 1987, PASP, 99, 191

Tanvir N. R., Levan A. J., Fruchter A. S., Hjorth J., Hounsell R. A., Wiersema K., Tunnicliffe R. L., 2013, Nature, 500, 547

Thöne C. C., et al., 2011, MNRAS, 414, 479

Tunnicliffe R. L., et al., 2014, MNRAS, 437, 1495

Vernet J., et al., 2011, A&A, 536, A105

Wallner A., et al., 2015, Nat. Commun., 6, 5956

Wanderman D., Piran T., 2015, MNRAS, 448, 3026

Watson D., et al., 2013, ApJ, 768, 23

Willingale R., Starling R. L. C., Beardmore A. P., Tanvir N. R., O'Brien P. T., 2013, MNRAS, 431, 394

Yang B., et al., 2015, Nat. Commun., 6, 7323

Zhang B., et al., 2009, ApJ, 703, 1696

de Blok W. J. G., Walter F., 2014, AJ, 147, 96

de Ugarte Postigo A., et al., 2006, ApJ, 648, L83

de Ugarte Postigo A., et al., 2011, A&A, 525, A109

de Ugarte Postigo A., et al., 2014, A&A, 563, A62

van de Voort F., Quataert E., Hopkins P. F., Kere D., Faucher-Giguere C.-A., 2014, MNRAS, 447, 140

van der Walt S., Colbert S. C., Varoquaux G., 2011, CSE, 13, 22

List of Objects